

Structure and Enantio-Differentiating Behaviors of Nickel(II) Complexes with Chiral Schiff Base Ligands Derived from 1,1′-Binaphthyl-2,2′-diamine

Mariko Saito,[1] Hisako Sato,[2,3,†] Yukie Mori,*[1,††] and Yutaka Fukuda[1]

[1]Department of Chemistry, Ochanomizu University, 2-1-1 Otsuka, Bunkyo-ku, Tokyo 112-8610

[2]Graduate School of Science, The University of Tokyo, 7-3-1 Hongo, Bunkyo-ku, Tokyo 113-0033

[3]PRESTO, Japan Science and Technology Agency, Chiyoda-ku, Tokyo 102-0075

Received May 13, 2009; E-mail: mori97@riken.jp

Crystal structures of nickel(II), copper(II), and palladium(II) complexes with (*R*)-/(*S*)-2,2′-bis(salicylideneamino)-1,1′-binaphthyl were determined. The nickel complex **1** is binuclear consisting of two Ni^{2+} ions and homochiral two ligand dianions in the crystal. Each Ni^{2+} ion has a *trans*-N_2O_2 square-planar coordination sphere. Either the metal ion or the ligand is less distorted in binuclear complex **1** as compared with the mononuclear copper(II) complex, which has an intermediate structure between square-planar and tetrahedral forms. When dissolved in solvent, complex **1** dissociates into mononuclear species. It is likely that crystallization involves partial ligand-exchange of a mononuclear complex with another molecule of the same chirality to form a homochiral dimer in a self-sorting fashion. Nickel complex with 2,2′-bis(4-methoxysalicylideneamino)-1,1′-binaphthyl (**2**) forms a 1:1 adduct with (*R*)-2-(1-hydroxyethyl)pyridine in chloroform solution. The binding constant of (*R*)-**2** is twofold higher than that of (*S*)-**2**, which means that the adduct formation proceeds with enantio-differentiation.

Chiral ligands such as camphor derivatives are often utilized to control the chirality of metal centers in coordination compounds.[1] A variety of chiral ligands are currently used as building blocks for architectures of chiral supramolecular systems with various shapes including helicates, boxes, and polyhedrons.[2] In some cases, formation of a chiral molecular assembly results from the self-sorting ability of the complex.[3,4]

Among chiral ligands developed to date, 1,1′-binaphthyl-2,2′-diamine (binam) derivatives have a unique feature in that their chirality results from restriction of rotation about the 1,1′-bond, that is, atropisomerism. A number of binam derivatives having coordination sites are reported[5,6] and some of them are used in asymmetric catalyst systems.[7–13] For example, metal complexes with salen-like Schiff base ligands derived from binam (e.g., H_2L in Figure 1) are used in various organic reactions.[9–13] This type of ligand normally coordinates as a tetradentate in non-planar geometry with helical twisting in either four-coordinated or six-coordinated complexes.[10,12,13] Only a palladium(II) complex [PdL($R^3 = R^5 = Cl$, $R^4 = H$)] is reported to adopt pseudo-square-planar geometry probably due to the strong preference of palladium(II) ion for a square-planar coordination.[11] Although crystal structures of a number of divalent and trivalent metal complexes of these ligands have been determined,[9–13] no X-ray structure analyses for nickel(II) complexes have been reported yet.

We have analyzed the X-ray crystal structure of racemic nickel(II) complex with L^1 (Figure 1). The crystal consists of binuclear complex [$Ni_2L^1_2$] containing two homochiral ligands each of which coordinates to two Ni atoms. The ability to bridge two metals may be of great importance for the binam-derived ligand since it has been proposed that two metal centers are involved in some metal-catalyzed reactions.[14] Indeed, binuclear complexes where two metals are placed in appropriate arrangement exhibit high catalytic activity.[15] In order to explain formation of the homochiral dimer, we compared the molecular structures among divalent metal complexes with L^1 including [CuL^1] (**3**) and [PdL^1] (**4**) and carried out DFT calculations for dimeric and monomeric models of the nickel(II) complex. Structures of complexes **1**–**4** in solution have been characterized by means of CD, UV–vis–NIR, NMR, and ESR spectrometries. Furthermore, enantio-differentiation was investigated in adduct formation for nickel(II) complex **2** with chiral donor molecules.

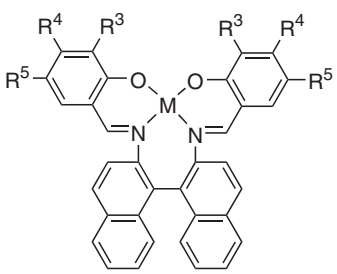

	M	R^3	R^4	R^5
H_2L^1	2H	H	H	H
H_2L^2	2H	H	OMe	H
[NiL^1] (**1**)	Ni	H	H	H
[NiL^2] (**2**)	Ni	H	OMe	H
[CuL^1] (**3**)	Cu	H	H	H
[PdL^1] (**4**)	Pd	H	H	H

Figure 1. Structures of ligands and complexes.

† Present address: Graduate School of Science and Engineering, Ehime University, Matsuyama 790-8577

†† Present address: RIKEN, 2-1 Hirosawa, Wako 351-0198

Published on the web October 8, 2009; doi:10.1246/bcsj.82.1266

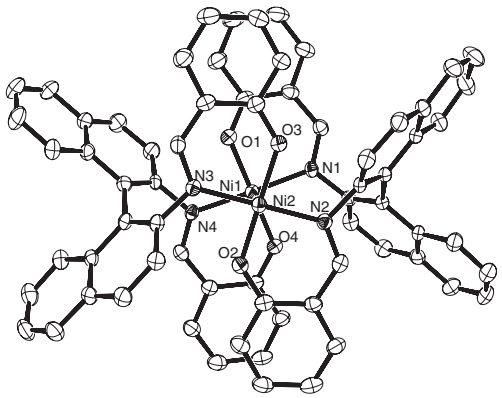

Figure 2. ORTEP diagram of complex **1**. The thermal ellipsoids enclose 30% probability. Hydrogen atoms are excluded for clarity.

Table 1. Selected Bond Distances (Å) and Angles (°) of *rac*-**1**

Ni(1)–O(1)	1.826(4)	Ni(2)–O(2)	1.825(4)
Ni(1)–O(4)	1.827(4)	Ni(2)–O(3)	1.825(4)
Ni(1)–N(1)	1.933(4)	Ni(2)–N(2)	1.921(5)
Ni(1)–N(4)	1.927(5)	Ni(2)–N(3)	1.927(5)
O(1)–Ni(1)–N(1)	93.0(2)	O(2)–Ni(2)–N(2)	92.6(2)
O(1)–Ni(1)–N(4)	86.6(2)	O(2)–Ni(2)–N(3)	88.2(2)
O(4)–Ni(1)–N(4)	93.3(2)	O(3)–Ni(2)–N(3)	92.7(2)
O(4)–Ni(1)–N(1)	87.3(2)	O(3)–Ni(2)–N(2)	86.8(2)
O(1)–Ni(1)–O(4)	177.7(2)	O(2)–Ni(2)–O(3)	176.8(2)
N(1)–Ni(1)–N(4)	173.0(2)	N(2)–Ni(2)–N(3)	175.2(2)

Results and Discussion

Crystal Structure of Nickel(II) Complex *rac*-1. The X-ray structure analysis for *rac*-**1** revealed that the molecule is a dimer $[Ni_2L^1{}_2]$ consisting of two Ni^{2+} ions and two homochiral ligand anions. The unit cell consists of a pair of (*R*,*R*)-$[Ni_2L^1{}_2]$ and (*S*,*S*)-$[Ni_2L^1{}_2]$ together with one benzene molecule, which lies on the crystallographic inversion center. Figure 2 shows the molecular structure of (*R*,*R*)-$[Ni_2L^1{}_2]$. Selected geometric parameters are listed in Table 1. Each nickel atom has a *trans*-N_2O_2 square-planar coordination sphere like bis(N-substituted salicylaldiminato)nickel(II). The nickel atoms are displaced from their coordination planes only by 0.041 and 0.012 Å, and the Ni(1)···Ni(2) distance is 3.033 Å. The two coordination planes are almost parallel, forming a small dihedral angle of 4.1° and rotated around the Ni(1)–Ni(2) axis against each other by ca. 37°. The two salicylidene units in each ligand are partially stacked with interplane distances of ca. 3.6 Å. The direction of rotation is determined by the chirality of the ligand: counterclockwise in the R,R dimer and vice versa. The Ni–N distances (1.921–1.933 Å) and Ni–O distances (1.825–1.827 Å) are normal values for square-planar nickel(II) complexes.

The benzene molecule does not show either π–π stacking or C–H···π interaction with the complex but only fills the void formed by the peripheral benzene rings. Inclusion of appropriate guests may help crystallization of molecules having rigid and bulky groups at their periphery, which would otherwise be difficult to crystallize. In the hemi-benzene solvate of **1**, inclusion of centrosymmetric benzene molecules may cause predominant crystallization of racemate over conglomerate.

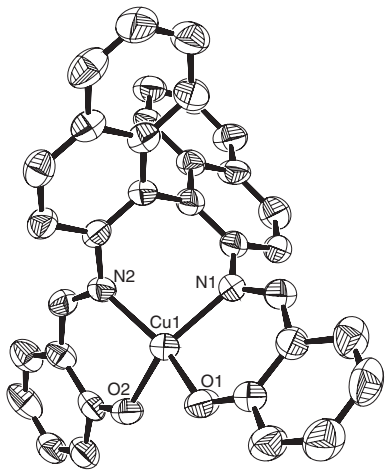

Figure 3. ORTEP diagram of complex **3**. The thermal ellipsoids enclose 30% probability. Hydrogen atoms are excluded for clarity.

Table 2. Selected Bond Distances (Å) and Angles (°) of (*R*)-**3** and *rac*-**4**

$[CuL^1]$ ((*R*)-**3**)		$[PdL^1]$ (*rac*-**4**)	
Cu(1)–O(1)	1.882(7)	Pd(1)–O(1)	1.997(2)
Cu(1)–O(2)	1.890(6)	Pd(1)–O(2)	1.988(2)
Cu(1)–N(1)	1.961(7)	Pd(1)–N(1)	2.008(2)
Cu(1)–N(2)	1.954(6)	Pd(1)–N(2)	2.012(2)
N(1)–Cu(1)–N(2)	97.4(3)	N(1)–Pd(1)–N(2)	94.6(1)
O(1)–Cu(1)–O(2)	90.6(3)	O(1)–Pd(1)–O(2)	84.8(1)
N(1)–Cu(1)–O(1)	92.9(3)	N(1)–Pd(1)–O(1)	88.8(1)
N(2)–Cu(1)–O(2)	92.9(3)	N(2)–Pd(1)–O(2)	92.7(1)
N(1)–Cu(1)–O(2)	149.9(3)	N(1)–Pd(1)–O(2)	170.6(1)
N(2)–Cu(1)–O(1)	152.9(3)	N(2)–Pd(1)–O(1)	171.1(1)

Structure of Copper(II) Complex (*R*)-3. Figure 3 shows the molecular structure of (*R*)-**3**. Selected bond distances and angles are listed in Table 2. The structure is quite similar to that observed in racemic crytal.[12] The dihedral angle between N(1)–Cu(1)–O(1) and N(2)–Cu(1)–O(2) planes is 39.6°, which is smaller than the corresponding angle for $[CoL^1]$ (71.9°)[13] but larger than that for $[PdL^1]$ (10.9°). The coordination geometry may be regarded as either flattened tetrahedral or twisted square-planar, that is, intermediate between these categorized structures.

The ESR spectrum of **3** in frozen tetrahydrofuran or chloroform showed an axial type signal with $g_{\parallel} = 2.25$ and $A_{\parallel} = 164.6 \times 10^{-4}\,cm^{-1}$ (Figure S1). The relatively large $A_{\parallel}$ value suggests that the electronic configuration of Cu^{2+} is close to that of a typical square-planar copper(II) complex.[16]

Structure of Palladium(II) Complex *rac*-4. The molecular structure of **4** is shown in Figure 4 and selected bond distances and angles are listed in Table 2. The coordination geometry of Pd^{2+} is pseudo square-planar, as is reported for a similar complex [PdL($R^3 = R^5 = Cl$, $R^4 = H$)].[11] The metal–ligand bonds are longer than those in the nickel(II) or

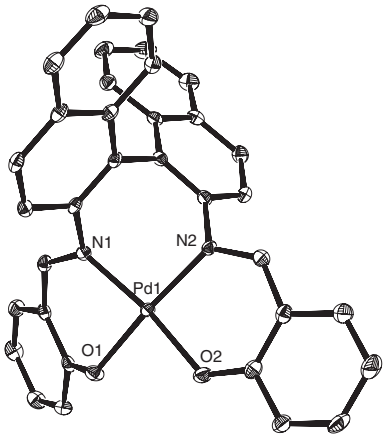

Figure 4. ORTEP diagram of complex **4**. The thermal ellipsoids enclose 50% probability. Hydrogen atoms are excluded for clarity.

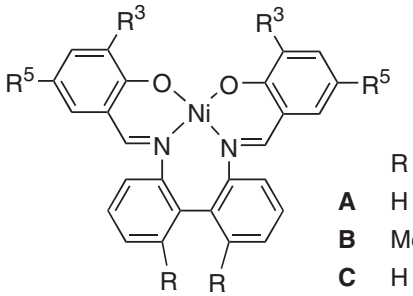

	R	R^3	R^5
A	H	*sec*-Bu	Me
B	Me	*sec*-Bu	Me
C	H	H	Me

Figure 5. Structures of related complexes **A**–**C** reported in Ref. 17.

copper(II) complex due to the larger ionic radius of Pd^{2+}. The ^{1}H NMR spectrum of **4** suggested that this complex exists in diamagnetic square-planar form in solution.

Solution Equilibria of Nickel Complexes 1 and 2. The coordination mode in $[Ni_2L^1{}_2]$ is novel for this ligand. It was reported that Mn^{3+} also forms a binuclear complex, $[Mn^{III}{}_2L^1{}_2(OMe)_2]$, but the two Mn^{3+} ions in this complex are bridged by MeO^- and the coordination mode of L^1 is different from that in **1**.[10] Holm et al. reported that similar nickel complexes (complexes **A**–**C** in Figure 5) exist as an equilibrium mixture of monomeric square-planar (Sp) and tetrahedral (Td) forms in solution even in relatively high concentrations.[17] Is the binuclear complex **1** intact or dissociated into monomers when it is dissolved in solvent? Low solubility of **1** at low temperature hampered cryoscopic determination of its molecular weight in solution. We instead tried to discriminate the dimer (MW 1098.5) and monomer (MW 549.2) by comparing retention times of a GPC column (Bio-Beads SX8, eluted with $CHCl_3$). Complex **1** was eluted as a single band at almost the same retention time as that of ZnL^1 (MW 555.9) while the internal standard (a blue-violet pigment; MW 983) was eluted at a shorter time. This result suggested that **1** exists as monomer $[NiL^1]$ rather than dimer $[Ni_2L^1{}_2]$ in $CHCl_3$ solution. To confirm this assumption, we examined spectral properties of **1** and **2** in solution, particularly concentration dependence.

The absorption spectrum of **1** in $CDCl_3$ exhibits a shoulder at 666 nm and a weak band at 1211 nm. This spectral feature is similar to that of [NiL(R^3 = *sec*-Bu, R^4 = H, R^5 = Me)].[17] The former absorption is assigned to the d–d transition of the Sp form while the latter to that of the Td form.[18,19] The dimer $[Ni_2L^1{}_2]$ also has a square-planar N_2O_2-coordination sphere and hence should exhibit a similar absorption band around 660 nm. However, the peak position or band shape may be slightly different from those of the monomer since the dimer has *trans*-N_2O_2 configuration while the monomer is *cis*-N_2O_2. If complex **1** were present as an equilibrium mixture of the monomer and dimer, the absorption spectra would vary with the concentration. The UV–vis–NIR spectrum of **1** in $CDCl_3$ showed no change in spectral shape, and the absorbance at 660 nm obeyed Beer's law in a concentration range of $(0.5–10) \times 10^{-3}$ mol dm^{-3}. Complex **2** also showed a similar absorption spectrum. The absorption peak due to the Sp form is 650 nm, indicating the ligand field of L^2 is stronger than that of L^1 due to the presence of electron-donating methoxy groups. No concentration dependence was observed in the UV–vis–NIR spectrum for **2**. The CD spectrum of enantiopure **1** or **2** (Figure S2) shows a couplet in the π,π^* absorption region of azomethine chromophore, which is similar to that of complexes **A**–**C** or other complexes with similar binaphthyl-linked Schiff base ligands.[17,20] In the ^{1}H NMR spectra of **1** and **2**, neither chemical shifts nor peak widths were concentration-dependent. From these results, we can conclude that **1** and **2** exist as monomeric forms in solution.

As mentioned above, both the Sp and Td forms are present in the solution of **1** or **2**. The fraction of Td form, x_{Td}, was estimated to be 0.15 for **1** or 0.12 for **2** in 1,1,2,2-tetrachloroethane at 298 K from the contact shift of ^{1}H NMR spectra. These values are similar to the x_{Td} values of complexes **A**–**C** in $CDCl_3$ at 298 K (0.07–0.15).[17]

Although no dimerization has been observed for either **1** or **2** in solution up to 1.0×10^{-2} mol dm^{-3}, the concentration of the complex may be much higher at the saturation point and hence a dimer may be formed and crystallize out from the solution probably due to solubility lower than that of the monomer. It should be noted that self-sorting of the ligand takes place to form the homochiral dimer. Although existence of a heterochiral dimer cannot be ruled out only from the structure observed for one crystal, consideration with molecular modeling suggests that formation of the heterochiral dimer, (*R*,*S*)-$[Ni_2L^1{}_2]$, is impossible due to steric repulsion of the ligands. Thus, the rigid framework of binaphthyl enables the ligand to discriminate itself from its antipode.

Comparison of Coordination Structure of L^1 among Various Metals. As has been demonstrated, ligand L^1 adopts various coordination modes according to the central metal. The geometric parameters for the cobalt(II), nickel(II), copper(II), and palladium(II) complexes are listed in Table 3. For square-planar mononuclear nickel complex $[NiL^1]$, the values of a model optimized at B3LYP/CEP-31G level of theory are given (Figure 6).

The dihedral angle between the N–M–O planes ($\phi_{N–M–O}$; where M denotes metal) decreases in the order: $[CoL^1] > [CuL^1] > [NiL^1] > [PdL^1] > [Ni_2L^1{}_2]$. The decrease of this angle means that the N_2O_2 coordination sphere changes from the Td to the Sp form. This trend indicates that the coordination structure is predominantly determined by the structural prefer-

Table 3. Geometric Parameters for Various Metal Complexes with L^1

	CoL^1 (293 K[b)])	CuL^1 (250 K)	NiL^1 (calcd[c)])	PdL^1 (90 K)	$Ni_2L^1{}_2$ (293 K)	$Ni_2L^1{}_2$ (calcd[c)])
M[a)]–O/Å	1.886, 1.904	1.882, 1.890	1.862	1.988, 1.997	1.825–1.827	1.851
M–N/Å	1.982, 1.978	1.954, 1.961	1.930	2.008, 2.012	1.921–1.933	1.970
N–M–O/°	94.3, 95.2	92.9, 92.9	92.2	88.8, 92.7	92.6–93.3	92.4
ϕ_{N-M-O}/°	71.9	39.6	18.4	10.9	7.3, 5.3	3.7
$\phi_{Nap-Nap}$/°	70.6	67.7	67.6	70.6	82.2, 73.7	76.8

a) M denotes metal. b) Ref. 13. c) By DFT calculation.

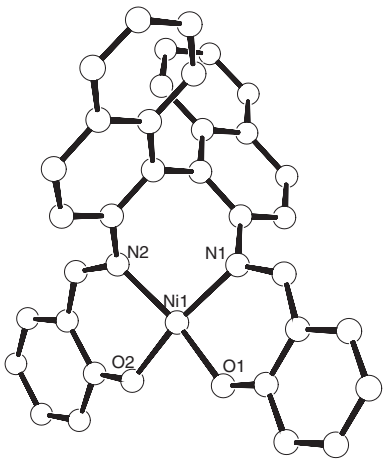

Figure 6. Optimized structure of the model of square-planar $[NiL^1]$. Hydrogen atoms are excluded for clarity.

ence of the metal ion. The dihedral angle between the two naphthalene planes ($\phi_{Nap-Nap}$) is 77.5° in free ligand H_2L^1.[21] The $\phi_{Nap-Nap}$ values in the mononuclear pseudo-Sp complexes are smaller, indicating that the ligand suffers from strain. In palladium(II) complex **4**, elongation of the metal–ligand bonds allows greater twisting of the binaphthyl unit even with higher planarity at the metal center, as compared with monomeric nickel(II) complex $[NiL^1]$.

The structure of dimer $[Ni_2L^1{}_2]$ is favorable for both the nickel(II) ion and ligand L^1: the N_2O_2-donor sets provide almost non-distorted Sp coordination to each nickel and the structural deviation of L^1 from its free state is minimized. DFT calculation predicts that $[Ni_2L^1{}_2]$ will be more stable than $[NiL^1]$ by $-3.56\,kJ\,mol^{-1}$ per NiL^1 unit (difference in the zero-point energy is not included). The π–π stacking of salicylidene planes in $[Ni_2L^1{}_2]$ may also stabilize the dimer (Figure 2). To discuss the relative stability in solution, solvation effects should be taken into consideration. Although chlorinated hydrocarbon solvents such as chloroform do not directly coordinate to the metal, some interaction with the ligand moiety may stabilize the complex. Since exposure to solvent is more significant and dipole moment is larger in the monomer than in the dimer, the solvation effect will be larger for the monomer.

Enantio-Differentiation in Adduct Formation of Complex 2. It is known that bis(*N*-alkylsalicylaldiminato)nickel(II) forms an adduct with donors such as pyridine.[22] Complexes **1** and **2** also formed mono- and bis-adducts with pyridine in $CDCl_3$ solution. In the first step, two absorption bands appeared in the NIR region, indicating formation of five-coordinated $[NiL^2(pyridine)]$.[23] Further addition of pyridine gave bis-adduct $[NiL^2(pyridine)_2]$, which exhibited a weak absorption band typical for octahedral nickel(II) complexes[24] (Figure S3). The formation constants for **2** are listed in Table 4. The details for data analysis are given in Experimental.

Table 4. Formation Constants of (*R*)-**2** and (*S*)-**2** with Additives and Absorption Maxima of the Adducts in $CDCl_3$ at 298 K

Additive	(*R*)-**2**		(*S*)-**2**		λ_{max}/nm
Pyridine	$\log\beta_1$	1.21 ± 0.06	$\log\beta_1$	1.25 ± 0.10	1000, 1400
	$\log\beta_2$	2.34 ± 0.10	$\log\beta_2$	2.23 ± 0.26	940
(−)-Nicotine	$\log\beta$	1.32 ± 0.04	$\log\beta$	1.30 ± 0.04	960, 1360
(*R*)-pyOH	$\log\beta$	1.66 ± 0.04	$\log\beta$	1.35 ± 0.02	975

When a chiral donor coordinates to either enantiomer of a chiral complex, a pair of diastereomers is formed. Since the formation constants of diastereomers are generally different, the adduct formation may take place enantioselectively. We examined the possibility of enantio-differentiation in reaction of **2** with chiral pyridine derivatives. When (−)-nicotine was added to (*R*)-**2** or (*S*)-**2** in $CDCl_3$, the variation of UV–vis–NIR spectrum (Figure S4) indicates that a five-coordinated mono-adduct $[NiL^2(nicotine)]$ was formed. In contrast to the addition of pyridine, no bis-adduct was observed even with a large excess of nicotine. The formation constant is essentially the same for (*R*)-**2** and (*S*)-**2**, indicating that the chiral center of nicotine is too far from the metal center to cause any difference in stability.

It is expected that interligand interaction will be larger in six-coordinated than in five-coordinated complexes. We chose (*R*)-2-(1-hydroxyethyl)pyridine (abbreviated as (*R*)-pyOH hereinafter) as a bidentate ligand. Figure 7a shows the variation of UV–vis–NIR spectrum for (*R*)-**2** on addition of (*R*)-pyOH. The observed spectral change in the NIR region was different from that observed on addition of either pyridine or nicotine. A new band appeared at 975 nm, indicating the formation of an octahedral complex. No five-coordinated species was detected. The titration data can be fit by assuming an equilibrium involving 1:1 adduct $[Ni\{(R)\text{-}L^2\}\{(R)\text{-pyOH}\}]$. As seen in Figure 7b, the formation constant for (*R*)-**2** is higher than that for (*S*)-**2**, indicating that $[Ni\{(R)\text{-}L^2\}\{(R)\text{-pyOH}\}]$ is more stable than $[Ni\{(S)\text{-}L^2\}\{(R)\text{-pyOH}\}]$. However, the ratio $\beta((R)\text{-}\mathbf{2})/\beta((S)\text{-}\mathbf{2})$ is 2.0, which corresponds to a difference in ΔG as small as $1.71\,kJ\,mol^{-1}$. It seems difficult to rationalize the observed preference with such a small energy difference.

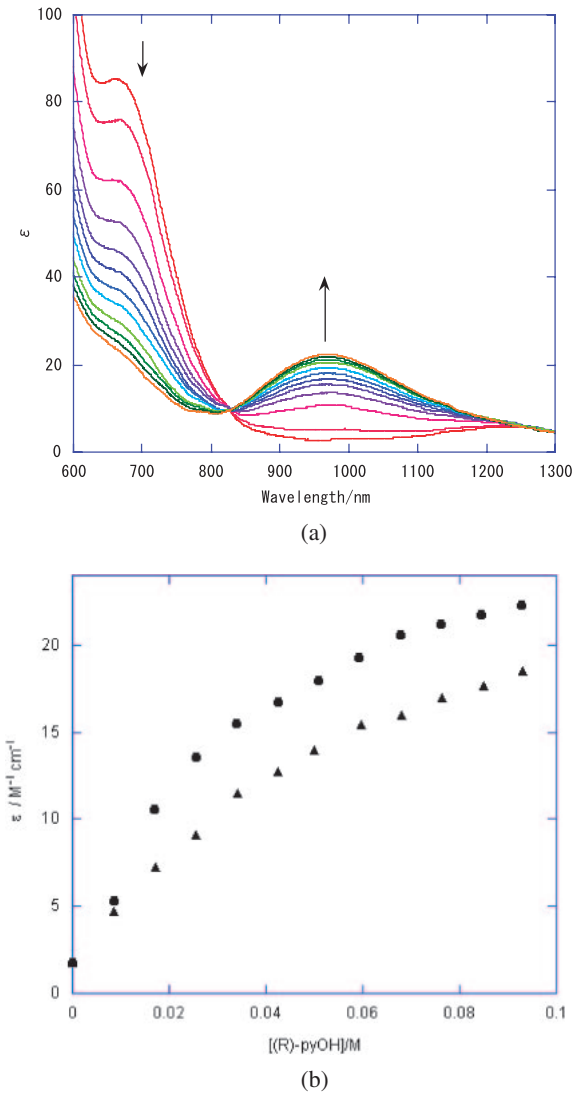

Figure 7. (a) Variation of UV–vis–NIR spectra of (*R*)-**2** in $CDCl_3$ on addition of (*R*)-pyOH. (b) Plots of molar extinction coefficient at 975 nm versus the concentration of (*R*)-pyOH for (*R*)-**2** (circle) and (*S*)-**2** (triangle) (At 298 K, concentration of **2**: 2.3×10^{-3} M).

Conclusion

In conclusion, 2,2′-bis(salicylideneamino)-1,1′-binaphthyl forms metal complexes with a variety of coordination modes. The coordination structure is determined by both the electronic configuration of metal and the degree of strain within the ligand caused on coordination. In mononuclear complexes with a small metal ion, both the metal and ligand tolerate some deficit. On the other hand, the binuclear nickel(II) complex, $[Ni_2L^1{}_2]$, satisfies the planarity of the N_2O_2-coordinatioin sphere and the strain-free conformation of the ligand at the same time. In solution, nickel complexes **1** and **2** exist mainly as the monomeric Sp form. Enantio-differentiating ability of the binam-derived Schiff base ligands is demonstrated in self-sorting dimerization of **1** and in the adduct formation with a chiral donor for (*R*)-**2** and (*S*)-**2**.

Experimental

The starting materials are commercially available and were used as received. Spectroscopic grade reagents and deuterated solvents were dried over Molecular Sieves 4A before use for measurement of absorption or ^{1}H NMR spectra. IR spectra were recorded on a Perkin-Elmer Spectrum2000 FT-IR spectrometer as KBr disks. FAB mass spectra were obtained with a JEOL JMS-700 Mstation with 3-nitrobenzyl alcohol as matrix. ^{1}H (400 MHz) and ^{13}C (100.4 MHz) NMR spectra were recorded on a JEOL JNM-AL-400 spectrometer. In ^{1}H NMR spectra, signals due to $CHCl_3$ (δ 7.26), $CHDCl_2$ (δ 5.30) or $CHCl_2CDCl_2$ (δ 5.91) were used as internal references, and in ^{13}C NMR, that of $CDCl_3$ (δ 77.0) was used. The UV–vis–NIR spectra were obtained on a Shimadzu UV3600PC spectrophotometer. X-band ESR spectra were recorded on a JEOL JES-FE2XG at 77 K. Thermal gravimetry and differential thermal analysis (TG-DTA) were performed on a Shimadzu DTA-50 thermal analyzer controlled by a Shimadzu TA-50WS system at a heating rate of 5 K min^{-1}. CD spectra were obtained at room temperature in $CHCl_3$ on a JASCO J-820 spectropolarimeter.

Synthesis of 1. A hot suspension of 2,2′-bis(salicylideneamino)-1,1′-binaphthyl[8a] (0.821 g, 1.67 mmol) in ethanol containing triethylamine (0.342 g, 3.38 mmol) was added dropwise to a hot ethanol solution of nickel acetate tetrahydrate (0.416 g, 1.67 mmol). The resultant mixture was heated under reflux overnight. The reaction mixture was evaporated under reduced pressure to leave brown residue, which was diluted with water and extracted with chloroform. The organic layer was concentrated and the crude product was purified by medium-pressure chromatography on silica gel using chloroform–methanol as eluent to yield **1** as brown powder (0.204 g, 30%). IR: 1609 cm^{-1} (νC=N); ^{1}H NMR ($C_2D_2Cl_4$, 298 K): δ 2.53 (2H, br t), 2.73 (2H, br), 6.35 (4H, m), 6.76 (2H, t, $J = 8$ Hz), 7.71 (2H, d, $J = 8$ Hz), 7.96 (2H, t, $J = 8$ Hz), 8.81 (2H, d, $J = 8$ Hz), 10.33 (2H, br d), 10.40 (2H, br); m/z (FAB) 1097 ($[Ni_2L^1{}_2 + H]^+$) and 549 ($[NiL^1 + H]^+$). TG-DTA and ^{1}H NMR data shows that the formula is $[NiL^1]\cdot 0.4CHCl_3$.

Single crystals of *rac*-**1** were obtained from a benzene solution containing an equimolar mixture of (*R*)-**1** and (*S*)-**1** by slow diffusion of ether vapor.

Synthesis of 2. 2,2′-Bis(4-methoxysalicylideneamino)-1,1′-binaphthyl, H_2L^2, was prepared by the same procedures as those for H_2L^1 using 4-methoxysalicylaldehyde. IR: 1606 cm^{-1} (νC=N); ^{1}H NMR ($CDCl_3$): δ 3.64 (6H, s), 6.11 (2H, d, $J = 8$ Hz), 6.28 (2H, t, $J = 8$ Hz), 7.03 (2H, d, $J = 8$ Hz), 7.11 (2H, d, $J = 8$ Hz), 7.19 (2H, t, $J = 8$ Hz), 7.38 (2H, t, $J = 8$ Hz), 7.51 (2H, d, $J = 8$ Hz), 7.89 (2H, d, $J = 8$ Hz), 8.00 (2H, d, $J = 8$ Hz), 8.45 (2H, s, CH=N), 12.59 (2H, s, OH); ^{13}C NMR ($CDCl_3$): δ 55.3 (OCH_3), 100.7, 106.8, 113.2, 116.8, 125.5, 126.3, 126.8, 128.1, 129.0, 129.7, 132.1, 133.2, 133.2, 143.5, 160.5, 163.3, 163.4; m/z (FAB) 553 ($[H_2L^2 + H]^+$).

Complex **2** was prepared by the same procedures as those for **1** using H_2L^2 instead of H_2L^1. Yield 17%. TG-DTA and ^{1}H NMR data shows that the formula is $[NiL^2]\cdot 0.3CHCl_3$. IR: 1612 cm^{-1} (νC=N); ^{1}H NMR ($C_2D_2Cl_4$, 298 K): δ 2.74 (2H, br d, $J = 8$ Hz), 3.44 (6H, s, OCH_3), 3.65 (2H, br s), 6.52 (4H, m), 6.78 (2H, t, $J = 8$ Hz), 7.06 (2H, d, $J = 8$ Hz), 7.82 (2H, t, $J = 8$ Hz), 8.66 (2H, d, $J = 8$ Hz), 9.93 (2H, d, $J = 8$ Hz), m/z (FAB) 609 ($[NiL^2 + H]^+$).

Synthesis of (*R*)-3.[12] A hot suspension of (*R*)-H_2L^1 (0.493 g, 1.00 mmol) in ethanol was added to a hot ethanol solution of copper(II) acetate monohydrate (0.200 g, 1.00 mmol), and the

Table 5. Crystal Data and Details for Structure Refinement

	rac-**1**·0.5benzene	(*R*)-**3**·0.5EtOH	*rac*-**4**
Crystal color	Brown	Blue	Orange
Crystal dimensions/mm^3	0.75 × 0.25 × 0.13	0.33 × 0.12 × 0.12	0.144 × 0.098 × 0.039
Crystal system	Triclinic	Tetragonal	Monoclinic
Space group	$P\bar{1}$	$P4_12_12$	$C2/c$
Formula	$C_{71}H_{47}N_4Ni_2O_4$	$C_{35}H_{25}CuN_2O_{2.5}$	$C_{34}H_{22}N_2O_2Pd$
Formula weight	1137.55	577.11	596.94
a/Å	8.712(3)	18.539(5)	21.621(2)
b/Å	13.507(2)		9.1290(7)
c/Å	24.593(3)	17.685(5)	26.021(3)
α/°	102.398(11)		
β/°	99.617(17)		100.328(2)
γ/°	98.191(18)		
V/Å^3	2738.5(10)	6078(3)	5052.8(8)
Z	2	8	8
μ/mm^{-1}	0.745	0.753	0.771
D_{calcd}/Mg m^{-3}	1.38	1.261	1.569
θ_{max}/°	25	26	25
T/K	293	250	90
Total reflections	8804	23205	41866
Unique reflections	8247	5956	4414
Observed reflections	6920	3783	4193
No. of parameters	731	360	440
R	0.0826	0.129	0.0275
R_w	0.140	0.316	0.0599
S	1.089	1.076	1.070

resultant solution was heated under reflux for 6 h. The reaction mixture was concentrated under reduced pressure, and the residue was diluted with water and extracted with benzene. The solvent was evaporated under reduced pressure to give dark green powder, which was recrystallized from chloroform (stabilized with 1% ethanol) to give **3** as dark blue fine needles (0.479 g, 80%). IR: 1607 cm^{-1} (νC=N); m/z (FAB) 554 ($[CuL^1 + H]^+$).

Synthesis of *rac*-4. A solution of *rac*-H_2L^1 (0.246 g, 0.50 mmol) and triethylamine (0.152 g, 1.5 mmol) in DMF was added to a DMF solution of $K_2[PdCl_4]$ (0.163 g, 0.50 mmol), and the resultant solution was stirred at room temperature overnight. The reaction mixture was slowly diluted with water in an ice bath to precipitate the desired complex. The orange solid was collected by centrifugation and dried to give *rac*-**4** (0.141 g, 47%). This solid was dissolved in chloroform and ether vapor was diffused into this solution to give crystals for X-ray structure analysis. IR: 1607 cm^{-1} (νC=N); ^{1}H NMR (CD_2Cl_2): δ 6.52 (2H, t, J = 8 Hz), 6.90 (2H, d, J = 8 Hz), 6.99 (2H, d, J = 8 Hz), 7.05 (2H, d, J = 8 Hz), 7.09 (2H, d, J = 8 Hz), 7.23 (4H, m), 7.30 (2H, s, CH=N), 7.45 (2H, t, J = 8 Hz), 7.88 (2H, d, J = 8 Hz), 7.93 (2H, d, J = 8 Hz); m/z (FAB) 596 ($[PdL^1 + H]^+$).

X-ray Structure Analysis. Data collection was performed using graphite-monochromatized Mo Kα radiation (λ = 0.71073 Å) on a MacScience M03XHF four-circle diffractometer for **1** or a Rigaku Saturn70 CCD diffractometer for **3** and **4**. The intensity data were corrected for Lorenz and polarization factors. Semiempirical absorption correction was applied for **1** using ψ-scan data while a numerical method was employed for **3** and **4**. The data reduction was carried out with maXus for **1** or CrystalClear[25] for **3** and **4**. The structure was solved by the direct method with SIR92[26] and refined by full-matrix least-squares with SHELXL97.[27] The non-H atoms were refined with anisotropic thermal parameters. For **1** and **3**, the H-atoms were included in the calculated positions with riding model. No H-atoms were included in the ethanol molecule contained in the crystal of **3**. The H-atoms in **4** were located on a difference map and refined with isotropic thermal parameters. For all the computation and drawings, WinGX package[28] was used. Crystal data and details for refinement are given in Table 5. Crystallographic data have been deposited with the Cambridge Crystallographic Data Centre: Deposition numbers CCDC-719457, CCDC-719456, and CCDC-719458 for **1**, **3**, and **4**, respectively. Copies of the data can be obtained free of charge via http://www.ccdc.cam.ac.uk/conts/retrieving.html (or from the Cambridge Crystallographic Data Centre, 12, Union Road, Cambridge, CB2 1EZ, U.K.; Fax: +44 1223 336033; e-mail: deposit@ccdc.cam.ac.uk).

Measurement of GPC Retention Times. A column packed with Bio-Beads SX8 (10 mm × 40 cm) was equilibrated with $CHCl_3$. Each sample dissolved in $CHCl_3$ containing an internal standard (blue-violet pigment $C_{60}H_{86}N_8O_4$, MW 983) was charged on the column and eluted with $CHCl_3$ at a flow rate of 0.6–0.7 cm^3 min^{-1}. The retention time, t_R, of **1** was 34 min when t_R of the standard was 30 min while t_R of ZnL^1 was 33 min when t_R of standard was 29 min.

Estimation of Fraction of Td Form. According to reported methods,[19] the fraction of Td form, x_{Td}, was determined from the chemical shift of 5-H for **1** and **2** at 298 K in 1,1,2,2-tetrachloroethane-d_2 at a concentration of 4×10^{-3} mol dm^{-3}. The chemical shift δ_{obs} is represented by eq 1 where δ_{dia} is the chemical shift of the diamagnetic form and δ_{con} is the contact shift, which is written by eq 2:

$$\delta_{obs} = \delta_{con} + \delta_{dia} \quad (1)$$

$$\delta_{con} = x_{Td} a(\gamma_e/\gamma_H) g\beta S(S+1)/(6SkT) \quad (2)$$

where *a* is the hyperfine coupling constant and the other symbols have their usual meanings. Here we used the chemical shift of the free ligand H_2L^1 or H_2L^2 as δ_{dia} and assumed that the *a* value should be equal to that of bis(*N-tert*-butylsalicylaldiminato)-nickel(II) for **1** or bis(*N-tert*-butyl-4-methylsalicylaldiminato)-nickel(II) for **2**.[19a]

Spectrophotometric Titration. All the experiments were performed at 298.0 ± 1.0 K using $CDCl_3$ as solvent. To a solution ($10\,cm^3$) of **2** [$(2.3–3.8) \times 10^{-3}$ mol dm^{-3}], a small aliquot of the additive was successively added and the UV–vis–NIR spectrum was recorded. For each experiment, more than 10 spectra were collected. Since the formation constants were not so high and the maximum molar absorption coefficients were much smaller for the five- or six-coordinated product than for the starting four-coordinated complex, we used a wide range of concentration up to a high $C_{additive}/C_{Ni}$ ratio. The formation constants and component spectra were determined by nonlinear least-squares fitting of the multi-spectral data using SPECFIT32[29] assuming the equilibria shown in eqs 3–5 for addition of pyridine, nicotine and pyOH, respectively.

$$[NiL^2] + \text{pyridine} \rightleftharpoons [NiL^2(\text{pyridine})](\text{five-coordinated}) \quad (3\text{-}1)$$

$$[NiL^2(\text{pyridine})] + \text{pyridine} \rightleftharpoons [NiL^2(\text{pyridine})_2](\text{six-coordinated}) \quad (3\text{-}2)$$

$$[NiL^2] + \text{nicotine} \rightleftharpoons [NiL^2(\text{nicotine})](\text{five-coordinated}) \quad (4)$$

$$[NiL^2] + \text{pyOH} \rightleftharpoons [NiL^2(\text{pyOH})](\text{six-coordinated}) \quad (5)$$

DFT Calculation. The DFT calculation was performed with B3LYP functional using Gaussian 03.[30] The dimer model with D_2 symmetry was constructed using the crystal structure and optimized with the basis sets of LANL2DZ for Ni and 6-31G* for the other atoms. The monomer model with C_2 symmetry was optimized by B3LYP/CEP-31G method. The single-point calculations were performed with the basis sets of 6-311G* for Ni, N, and O and 6-31G* for C and H. The computations were carried out at the Computer Center at the Institute of Molecular Science.

The authors are indebted to Professor Akihiko Yamagishi, Ochanomizu University, for fruitful discussion. Thanks are also due to Professor Makoto Chikira, Chuo University, and Dr. Daisuke Hashizume, RIKEN, for their help with measurement of ESR spectra and X-ray diffraction data, respectively.

Supporting Information

ESR spectrum of **3**, CD spectra of **1** and **2**, and spectral variation on titration. This material is available free of charge on the web at http://www.csj.jp/journals/bcsj/.

References

1 D. Shirotani, T. Suzuki, S. Kaizaki, *Inorg. Chem.* **2006**, *45*, 6111; G. W. Everett, Jr., R. M. King, *Inorg. Chem.* **1972**, *11*, 2041; R. M. King, G. W. Everett, Jr., *Inorg. Chem.* **1971**, *10*, 1237.

2 S. J. Lee, W. Lin, *Acc. Chem. Res.* **2008**, *41*, 521; J. Hamblin, L. J. Childs, N. W. Alcock, M. J. Hannon, *J. Chem. Soc., Dalton Trans.* **2002**, 164.

3 T. Iihoshi, T. Sato, M. Towatari, N. Matsumoto, M. Kojima, *Bull. Chem. Soc. Jpn.* **2009**, *82*, 458, and references therein.

4 M. Hutin, C. J. Cramer, L. Gagliardi, A. R. M. Shahi, G. Bernardinelli, R. Cerny, J. R. Nitschke, *J. Am. Chem. Soc.* **2007**, *129*, 8774.

5 S. G. Telfer, T. Sato, T. Harada, R. Kuroda, J. Lefevre, D. B. Leznoff, *Inorg. Chem.* **2004**, *43*, 6168; S. G. Telfer, R. Kuroda, *Coord. Chem. Rev.* **2003**, *242*, 33; G. Zi, L. Xiang, Y. Zhang, Q. Wang, X. Li, Y. Yang, Z. Zhang, *J. Organomet. Chem.* **2007**, *692*, 3949.

6 A. V. Wiznycia, J. Desper, C. J. Levy, *Dalton Trans.* **2007**, 1520; D. Prema, A. V. Wiznycia, B. M. T. Scott, J. Hilborn, J. Desper, C. J. Levy, *Dalton Trans.* **2007**, 4788.

7 C. M. Che, J. S. Huang, *Coord. Chem. Rev.* **2003**, *242*, 97.

8 a) H. Suga, A. Kakehi, S. Ito, H. Sugimoto, *Bull. Chem. Soc. Jpn.* **2003**, *76*, 327. b) Z. Chen, H. Morimoto, S. Matsunaga, M. Shibasaki, *J. Am. Chem. Soc.* **2008**, *130*, 2170.

9 C.-W. Ho, W.-C. Cheng, M.-C. Cheng, S.-M. Peng, K.-K. Cheng, C.-M. Che, *J. Chem. Soc., Dalton Trans.* **1996**, 405.

10 M.-C. Cheng, M. C.-W. Chan, S.-M. Peng, K.-K. Cheung, C.-M. Che, *J. Chem. Soc., Dalton Trans.* **1997**, 3479.

11 X.-G. Zhou, J.-S. Huang, X.-Q. Yu, Z.-Y. Zhou, C.-M. Che, *J. Chem. Soc., Dalton Trans.* **2000**, 1075.

12 Y. Wang, T. D. P. Stack, *J. Am. Chem. Soc.* **1996**, *118*, 13097.

13 Y.-M. Shen, W.-L. Duan, M. Shi, *J. Org. Chem.* **2003**, *68*, 1559.

14 For example: J. Park, K. Lang, K. A. Abboud, S. Hong, *J. Am. Chem. Soc.* **2008**, *130*, 16484.

15 B. A. Rodriguez, M. Delferro, T. J. Marks, *J. Am. Chem. Soc.* **2009**, *131*, 5902.

16 The $g_\parallel/A_\parallel$ value of **3** is 137 (cm), which is close to the usual range ($g_z/A_z = 105–135$ cm) for square-planar copper(II) complexes. P. Antunes, R. Delgado, M. G. B. Drew, V. Félix, H. Maecke, *Inorg. Chem.* **2007**, *46*, 3144.

17 M. J. O'Connor, R. E. Ernst, R. H. Holm, *J. Am. Chem. Soc.* **1968**, *90*, 4561.

18 L. Sacconi, M. Ciampolini, *J. Am. Chem. Soc.* **1963**, *85*, 1750.

19 a) A. Chakravorty, R. H. Holm, *J. Am. Chem. Soc.* **1964**, *86*, 3999. b) L. Sacconi, P. Nannelli, U. Campigli, *Inorg. Chem.* **1965**, *4*, 818. c) R. H. Holm, A. Chakravorty, G. O. Dudek, *J. Am. Chem. Soc.* **1964**, *86*, 379.

20 H. Sakiyama, H. Ōkawa, N. Oguni, T. Katsuki, R. Irie, *Bull. Chem. Soc. Jpn.* **1992**, *65*, 606.

21 J. Gao, J. H. Reibenspies, R. A. Zingaro, F. R. Woolley, A. E. Martell, A. Clearfield, *Inorg. Chem.* **2005**, *44*, 232.

22 R. Warmuth, H. Elias, *Inorg. Chem.* **1991**, *30*, 5027; M. Schumann, H. Elias *Inorg. Chem.* **1985**, *24*, 3187.

23 L. Sacconi, *Electronic Structure and Stereochemistry of Ni(II)*, in *Transition Metal Chemistry*, Marcel Dekker, Inc., New York, **1968**, Vol. 4.; N. Shintani, E. Nukui, H. Miyamae, Y. Fukuda, K. Sone *Bull. Chem. Soc. Jpn.* **1994**, *67*, 1828.

24 M. Arakawa, N. Suzuki, S. Kishi, M. Hasegawa, K. Satoh, E. Horn, Y. Fukuda, *Bull. Chem. Soc. Jpn.* **2008**, *81*, 127.

25 *CrystalClear*, Rigaku/MSC, The Woodland, Texas, USA.

26 A. Altomare, G. Cascarano, C. Giacovazzo, A. Guagliardi, M. C. Burla, G. Polidori, M. Camalli, *J. Appl. Crystallogr.* **1994**, *27*, 435.

27 G. M. Sheldrick, *SHELXL97, Program of the Refinement of Crystal Structures*, University of Göttingen, Germany, **1997**.

28 L. J. Farrugia, *J. Appl. Crystallogr.* **1999**, *32*, 837.

29 H. Gampp, M. Maeder, C. J. Meyer, A. D. Zuberbühler, *Talanta* **1985**, *32*, 95; H. Gampp, M. Maeder, C. J. Meyer, A. D. Zuberbühler, *Talanta* **1985**, *32*, 251.

30 M. J. Frisch, G. W. Trucks, H. B. Schlegel, G. E. Scuseria, M. A. Robb, J. R. Cheeseman, J. A. Montgomery, Jr., T. Vreven, K. N. Kudin, J. C. Burant, J. M. Millam, S. S. Iyengar, J. Tomasi,

V. Barone, B. Mennucci, M. Cossi, G. Scalmani, N. Rega, G. A. Petersson, H. Nakatsuji, M. Hada, M. Ehara, K. Toyota, R. Fukuda, J. Hasegawa, M. Ishida, T. Nakajima, Y. Honda, O. Kitao, H. Nakai, M. Klene, X. Li, J. E. Knox, H. P. Hratchian, J. B. Cross, C. Adamo, J. Jaramillo, R. Gomperts, R. E. Stratmann, O. Yazyev, A. J. Austin, R. Cammi, C. Pomelli, J. W. Ochterski, P. Y. Ayala, K. Morokuma, G. A. Voth, P. Salvador, J. J. Dannenberg, V. G. Zakrzewski, S. Dapprich, A. D. Daniels, M. C. Strain, O. Farkas, D. K. Malick, A. D. Rabuck, K. Raghavachari, J. B. Foresman, J. V. Ortiz, Q. Cui, A. G. Baboul, S. Clifford, J. Cioslowski, B. B. Stefanov, G. Liu, A. Liashenko, P. Piskorz, I. Komaromi, R. L. Martin, D. J. Fox, T. Keith, M. A. Al-Laham, C. Y. Peng, A. Nanayakkara, M. Challacombe, P. M. W. Gill, B. Johnson, W. Chen, M. W. Wong, C. Gonzalez, J. A. Pople, *Gaussian 03 Rev. D.01*, Gaussian, Inc., Pittsburgh PA, **2003**.